Monte Carlo simulations of atomic layer deposition on 3D large surface area structures: Required precursor exposure for pillar- versus hole-type structures

Véronique Cremers, Filip Geenen, Christophe Detavernier, and Jolien Dendooven

---

Monte Carlo simulations of atomic layer deposition on 3D large surface area structures: Required precursor exposure for pillar- versus hole-type structures

Véronique Cremers, Filip Geenen, Christophe Detavernier, and Jolien Dendooven[a)]

Department of Solid State Sciences, Ghent University, Krijgslaan 281/S1, Ghent 9000, Belgium

Due to its excellent conformality, atomic layer deposition (ALD) has become a key method for coating and functionalizing three dimensional (3D) large surface area structures such as anodized alumina (AAO), silicon pillars, nanowires, and carbon nanotubes. Large surface area substrates often consist of arrays of quasi-one-dimensional holes (into which the precursor gas needs to penetrate, e.g., for AAO), or "forests" of pillars (where the precursor gas can reach the surface through the empty 3D space surrounding the pillars). Using a full 3D Monte Carlo model, the authors compared deposition onto an infinite array of holes versus an infinite array of pillars. As expected, the authors observed that the required exposure to conformally coat an array of holes is determined by the height to width ratio of the individual holes, and is independent of their spacing in the array. For the pillars, the required exposure increases with decreasing center-to-center distance and converges in the limit to the exposure of an array of holes. Our simulations show that, when targeting a specific surface area enhancement factor in the range 20–100, a well-spaced pillar geometry requires a 2–30 times smaller precursor exposure than a hole geometry and is therefore more ALD friendly. The difference in required exposure is shown to depend on the initial sticking probability and structural dimensions. © *2016 American Vacuum Society.*
[http://dx.doi.org/10.1116/1.4968201]

I. INTRODUCTION

Large surface areas can be attained by introducing 3D structures such as anodized alumina membranes (AAO), silicon pillars, nanowires, and carbon nanotubes. Often these 3D nano- and microstructured large surface area substrates have to be functionalized, and therefore, atomic layer deposition (ALD) is an excellent method. Due to the self-limiting nature of the gas–solid surface reactions in ALD, it is possible to grow uniform thin films with a precise thickness control even in structures with high aspect ratios.[1–6] Examples of successful ALD-based functionalization of surface area enhanced (SAE) structures include the protection of semiconductor nanorods against contamination and oxidation,[7] the photo-activation of AAO or carbon nanosheet structures by coating with TiO_2,[8,9] and the deposition of a cathode material on aluminum nanorods used as current collector in Li-ion batteries.[10,11]

To have a better insight in the deposition process and to optimize the process parameters, several analytical and simulation models have been developed to describe the conformal ALD deposition in high aspect ratio structures. Among those, 2D models have been proposed to simulate thermal[12–20] and plasma-enhanced ALD in trenches.[21–23] This paper introduces a full 3D MC model, enabling simulation of thermal ALD processes in 3D structures. The model is applied here to compare ALD in an array of holes versus an array of pillars. Both, the holes and the pillars have a square cross section. The simulations provide insights in the exposure required to conformally coat the structures as a function of the hole/pillar dimensions and spacing between the holes/pillars. For a given SAE factor, our MC model shows that the pillar geometry requires a lower precursor dose, thus offering an important benefit toward the ALD-based functionalization of large surface area structures.

II. MODEL DESCRIPTION AND SIMULATION

A. 3D Monte Carlo simulations

To be able to compare ALD on different 3D substrates, we developed a full 3D MC model that describes the transport of precursor molecules, represented as MC particles, to the solid surface, followed by either reaction with the surface or reemission from the surface. In this model, we assume a molecular flow regime where particle–particle interactions can be neglected. This assumption is justified as long as the dimensions of the holes/opening between the pillars are much smaller than the mean free path of the precursor molecules. Therefore, this model is mostly relevant for low-pressure ALD in flow and pump-type reactors, for which a molecular flow regime can be obtained in micro- and nano-structured surfaces. In contrast, for atmospheric pressure ALD, the mean free path is only of the order of tens of nanometers and particle–particle scattering should be taken into account. In the MC model, the 3D structures are made up of planes discretized into square cells of equal surface area. For the infinite arrays of holes/pillars considered here, the symmetry is exploited to limit the simulation domain to a unity cell of one hole/pillar with periodic boundary conditions (MC particles that exit the simulation domain at a periodic boundary reenter at the equivalent position on the opposite boundary). The hole and pillar geometries are characterized

[a)]Electronic mail: jolien.dendooven@ugent.be

by a square cross section with width w, a height H, and a center-to-center distance D (Fig. 1). During the simulations, the width is kept constant, and the substrate geometry is varied by changing the H/w ratio and/or the D/w ratio. For holes, the H/w ratio is often termed the aspect ratio. Note that for each combination of H/w and D/w, the coatable surface area is equal for the array of pillars and the array of holes.

The principle of the model is similar to the earlier reported 2D models.[12–23] At the start of the simulation, a MC particle is generated at a random position in a horizontal "source plane" positioned above the top surface of the 3D structures. The MC particle is emitted with a cosine-distributed random direction and its trajectory is calculated. Once the intersection point with the 3D structure is determined, a random number r between 0 and 1 is generated to decide if the MC particle chemisorbs or desorbs. If $r < s_0(1 - \theta)$ with s_0 the initial sticking coefficient and θ the surface coverage of the corresponding discretization cell, the MC particle chemisorbs, i.e., the coverage θ is incremented, and a new MC particle is generated at the source plane. Otherwise, the MC particle desorbs and is emitted from the surface with a random direction defined by a cosine distribution. The algorithm is repeated until the MC particle chemisorbs or leaves the simulation domain through the top boundary. The generation of new MC particles is continued until the stop condition is fulfilled and the simulation ends. This condition can either be a predefined number of simulated particles or a predefined percentage of coated surface area of the substrate. The number of simulated MC particles, $N_{\text{simulated}}$, is then proportional to the precursor exposure needed to achieve the stop coverage. More specific, the relation between the exposure, defined as the product of the precursor partial pressure P and the precursor pulse time t, and $N_{\text{simulated}}$ is given by

$$\text{Pt} = K_{\max}\sqrt{2\pi mkT}\left[\frac{A_{\text{cell}}}{N_{\max,\text{cell}}}\frac{N_{\text{simulated}}}{A_{\text{source plane}}}\right]. \tag{1}$$

Herein, $K_{\max}$ is the maximum number of chemisorbed precursor molecules per unit area, m is the mass of the precursor

molecules, k is the Boltzmann constant, T is the temperature, A_{cell} is the surface area of a discretization cell, $N_{\max,\text{cell}}$ is the maximum number of chemisorbed MC particles in a discretization cell, and $A_{\text{source plane}}$ is the surface area of the source plane. In this expression, $K_{\max}\sqrt{2\pi mkT}$ equals the exposure needed for saturation of a flat surface.[9] Therefore, the factor within the brackets gives the normalized exposure, i.e., the factor by which the exposure, required to saturate a flat surface, must be increased to achieve the stop coverage of the array of holes or pillars. Note that this factor is independent of the choice of the precursor and deposition temperature. In this work, the simulation results are expressed in terms of both normalized and absolute exposures. The latter ones are calculated for trimethyl-aluminum (TMA), one of the most well-studied ALD precursors, at 200 °C. The absolute exposure is expressed in Langmuir (1 L = 10^{-6} Torr s).

B. Analytic approximations

With the aim to verify our 3D MC model, we derive in this section analytic approximation formulae for the normalized exposure required to saturate an array of holes and pillars, inspired by the work of Gordon *et al.*[12] and Yazdani *et al.*[24]

We assume a molecular flow regime, and therefore, the effective diffusion coefficient D_k in a cylindrical hole with pore diameter d_{pore} can be described by the Knudsen diffusivity[25]

$$D_k = d_{\text{pore}}\sqrt{\frac{8kT}{9\pi m}}, \tag{2}$$

with k the Boltzmann constant, T the temperature, and m the mass of the precursor molecules. This formula is, in principle, only valid for cylindrical holes with an infinite depth and should be multiplied with the Clausing factor for holes with a finite depth.[26] However, to allow for a straightforward modification of this formula for other geometries, as done below, the uncorrected formula (2) was used in this work. For holes with a square cross section defined by the width w, the diffusivity can be estimated as[27]

$$D_k = w\sqrt{\frac{8kT}{9\pi m}}. \tag{3}$$

For pillars with a square cross section defined by the width w, we estimate the diffusivity by replacing d_{pore} in Eq. (2) by the average open space between the pillars

$$D_k = \sqrt{2}\,(D - w)\sqrt{\frac{8kT}{9\pi m}}. \tag{4}$$

Herein, D is the pillar center-to-center distance.

Fick's law gives the precursor diffusion flux at a depth x in the hole/pillar array as

$$J = D_k \frac{n_{\text{chamber}}}{x}, \tag{5}$$

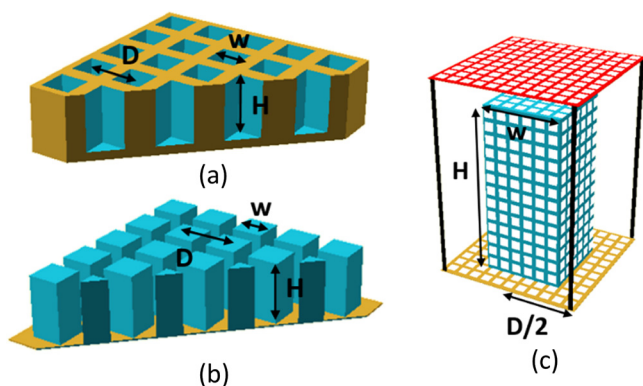with n_{chamber} the precursor concentration in the deposition chamber.

FIG. 1. (Color online) Array of holes (a) and pillars (b) with width w, height H, and center-to-center distance D and an example of a simulated unity cell of a pillar (c) built up of discretized interacting walls with in red the source plane.

Using the ideal gas law, we can rewrite this as

$$J = \frac{D_k P}{kTx}, \tag{6}$$

with P the precursor pressure in the chamber.

In analogy with the analytical derivation of Gordon *et al.*,[12] a sticking probability of 1 is assumed for the ALD precursor molecules diffusing into the hole/pillar array, implying that they will react upon their first collision with an unsaturated part of the substrate walls. When a molecule propagates along a saturated part, the sticking probability is 0. Based on these assumptions, the increment of time dt needed to coat an additional length dx of the hole/pillar structure is given by

$$dt = \frac{K_{\max} \, \Delta A_s}{J \, \Delta V} dx, \tag{7}$$

with $K_{\max}$ the saturated surface concentration of adsorbed precursor molecules or adsorption site density, ΔA_s the coatable surface area, and ΔV the void volume per unit volume of the hole/pillar structure.

Substitution of Eq. (6) in Eq. (7) allows us to write

$$P \, dt = K_{\max} \, kT \, \frac{\Delta A_s}{D_k \, \Delta V} x \, dx. \tag{8}$$

The diffusivity D_k for the holes and pillars can furthermore be generalized as $D_k = D'_k \sqrt{8kT/9\pi m}$ [see Eqs. (3) and (4)], so that Eq. (8) can be rewritten as

$$\frac{P}{K_{\max} \sqrt{2\pi m kT}} \, dt = \frac{3 \, \Delta A_s}{4 \, D'_k \, \Delta V} x \, dx. \tag{9}$$

Integration up to a time t at which the ALD front reaches a depth H of the hole/pillar structure (i.e., for $x = H$) gives an analytical expression for the normalized exposure required to coat the side walls of the hole/pillar structures until the depth H

$$\frac{Pt}{K_{\max} \sqrt{2\pi m kT}} = \frac{3 \, \Delta A_s \, H^2}{8 \, D'_k \, \Delta V}. \tag{10}$$

In the left hand side, one recognizes the expression of the normalized exposure. For the array of holes: $\Delta A_s = \sigma_{\text{hole}} 4w = 4w/D^2$, $\Delta V = \sigma_{\text{hole}} w^2 = w^2/D^2$, $D'_k = w$ with σ_{hole} the areal density of the holes and the expression reduces to

$$\frac{Pt}{K_{\max} \sqrt{2\pi m kT}} = \frac{3}{2} \left(\frac{H}{w} \right)^2. \tag{11}$$

For the array of pillars: $\Delta A_s = \sigma_{\text{pillar}} 4w = 4w/D^2$, $\Delta V = 1 - \sigma_{\text{pillar}} w^2 = 1 - (w^2/D^2)$, $D'_k = (D - w)$ with σ_{pillar} the areal density of the pillars and expression (10) reduces to

$$\frac{Pt}{K_{max} \sqrt{2\pi m kT}} = \frac{3 \left(\dfrac{H}{W} \right)^2}{2 \left(\dfrac{D}{w} - 1 \right) \left(\dfrac{D^2}{w^2} - 1 \right)}. \tag{12}$$

With these expressions, one can estimate the normalized exposure required to cover an array holes or pillars to a given depth H. As any real ALD process will have a sticking probability of less than 1, the obtained values should be considered as lower limits to the actual required exposures.[12] For the field of holes, the required exposure time depends, as expected,[12] quadratically on the hole aspect ratio and is independent of the density of holes. In case of the pillars, we remark not only a dependency on the depth to width ratio of the pillars but also on the density.

Using these formulae, we calculated the normalized saturation exposure for arrays of holes and pillars with $D/w = 3$ and compared these results with the values obtained using our 3D MC model. Figure 2 shows the results as a function of H/w. Except for small ratios of H/w, we found a good agreement between the MC and analytic results, confirming the validity of our MC model. The deviations at small H/w are likely explained by simplification of the diffusivity approximations in the analytic derivation.

III. RESULTS AND DISCUSSION

In this section, we will discuss the simulation results on arrays of holes and pillars with a square cross section, obtained with our 3D MC model. Figure 3 displays the TMA exposure required to achieve 90% coverage of an array of holes (a) and pillars (b) with varying ratios of H/w (x-axis) and D/w (y-axis). The absolute exposure is indicated as a logarithmic color scale. Note that, by expressing our results as a function of dimensionless geometry units, both microsized and nanosized structures fit on the same graphs. The color plot in Fig. 3(a) clearly indicates that the required exposure for an array of holes is determined by the ratio H/w of the individual holes, and is independent of their spacing D (or D/w) in the array. This is an expected result that is in agreement with the analytic formula mentioned above. In contrast, the analytic expression for an array of pillars shows a dependency on both the H/w and D/w ratios, and this is clearly reflected in the color plot in Fig. 3(b). The required exposure dose increases with decreasing pillar spacing D and converges in the limit of small D ($D/w < 1.5$) to the
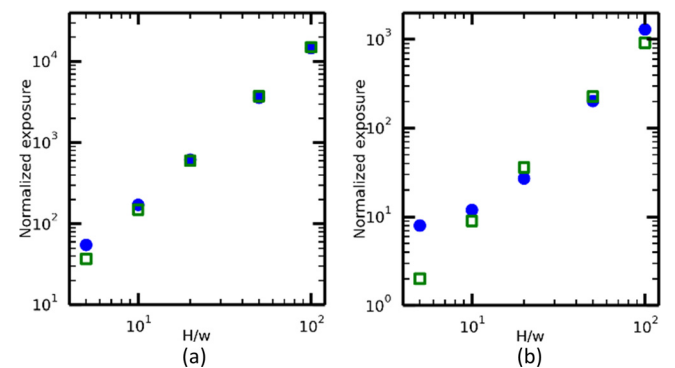

FIG. 2. (Color online) Calculated normalized exposure required to saturate arrays of holes (a) and pillars (b) with $D/w = 3$ and $H/w = 5$, 10, 20, 50, or 100: 3D Monte Carlo simulations with $s_0 = 1$ and stop coverage of 99% (blue circles) vs analytic approximation formulae (green squares).
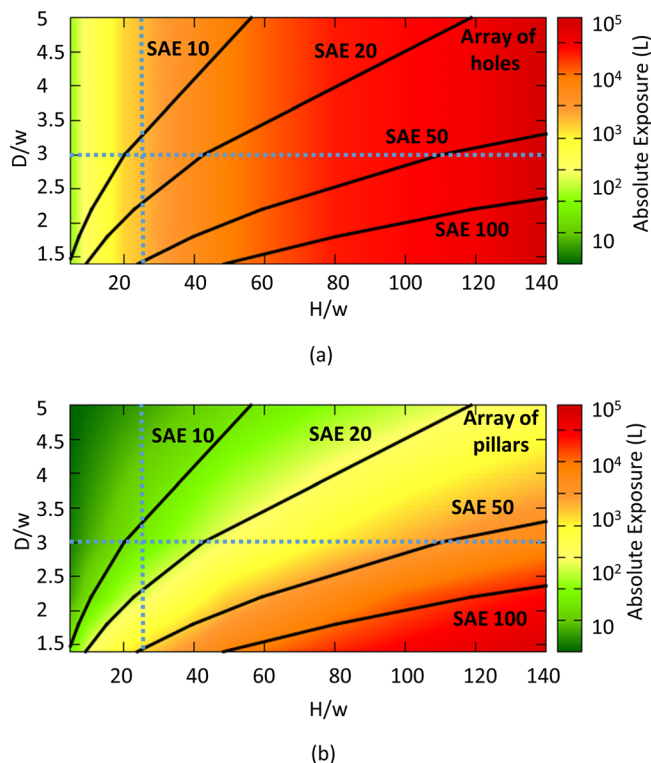
FIG. 3. (Color online) Required TMA exposure expressed on a logarithmic color scale as a function of the H/w and D/w ratio of arrays of holes (a) and pillars (b). The black contour lines indicate structures that result in SAE factors of 10, 20, 50, and 100. The 3D MC simulations used $s_0 = 1$ and stop coverage = 90%. The dashed vertical/horizontal lines mark the positions of the cross sections shown in Figs. 4 and 5. The absolute exposure on a flat substrate for given parameters is equal to 2.47 L.

FIG. 4. (Color online) Cross section along the dashed vertical lines in the color plots in Fig. 3 (data points for $s_0 = 1$ and stop coverage = 90%). Required TMA exposure (left y-axis) and normalized exposure (right y-axis) as a function of the D/w ratio of arrays of holes (green circles) and pillars (blue squares) with a fixed H/w ratio of 25.

exposure of an array of holes. This converging behavior is clearer in Fig. 4, where we plot the absolute (left y-axis) and normalized (right y-axis) exposure against D/w for a fixed H/w ratio of 25. By decreasing the center-to-center distance of the pillars, the empty space between the pillars becomes narrower and, for nearly touching pillars, starts to act as a 1D holelike structure, hence the similarity in required exposure.

For each H/w and D/w combination, the factor of surface area enhancement (SAE) compared to a flat surface can be calculated. The black contour lines in Fig. 3 indicate structures that share the same SAE factor. Except in the small D/w limit, the exposure required to reach a specific SAE is smaller for arrays of pillars than for arrays of holes. For example, when targeting a SAE factor of 50, the combination of $H/w = 110$ and $D/w = 2$ requires a ten times larger exposure for the hole geometry compared to the pillar geometry. For hole-type arrays, we remark that to achieve a certain SAE factor, it is more favorable to use short features (small H/w ratio) that are spaced very close to each other (small D/d ratio) than tall features (large H/w ratio) that are spaced farther apart from each other. In contrast, the required exposure is independent of the H/w and D/w combination for pillar-type arrays with a specific SAE factor. Figure 5 shows a cross section through the color plots in Fig. 3 at $D/w = 3$ and clearly illustrates that ALD of arrays of pillars requires
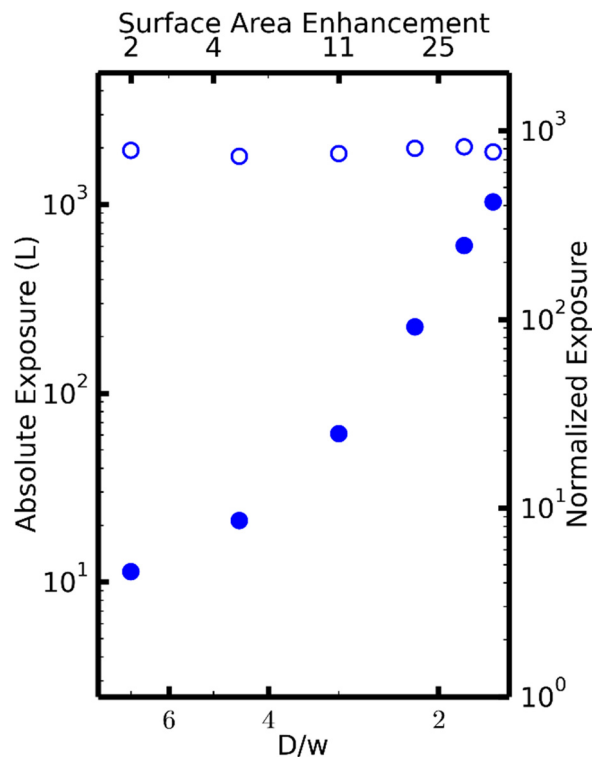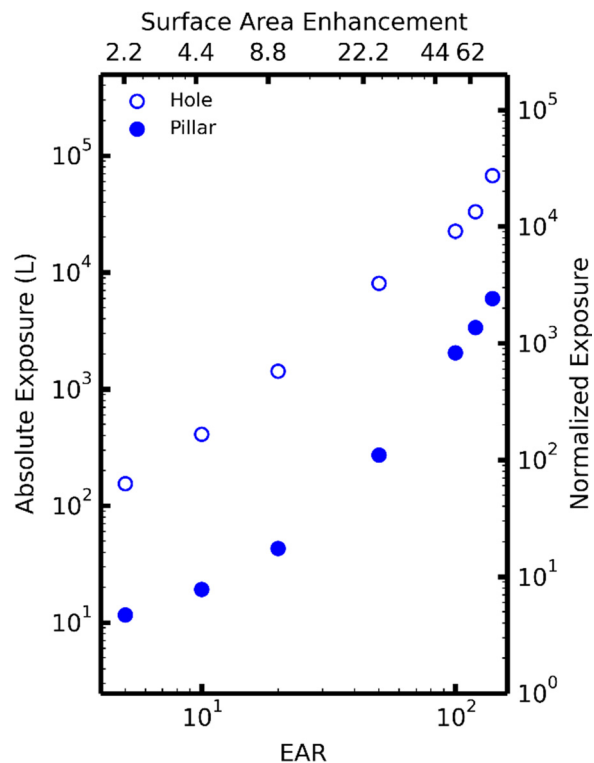

FIG. 5. (Color online) Cross section along the dashed horizontal lines in the color plots in Fig. 3 (data points for $s_0 = 1$ and stop coverage = 90%). Required TMA exposure (left y-axis) and normalized exposure (right y-axis) as a function of the H/w ratio of arrays of holes and pillars with a fixed D/w ratio of 3.

10 times less exposure as compared to arrays of holes for a whole range of SAE factors (top x-axis).

The effect of the initial sticking probability[28] on the calculated exposure times was investigated for both the hole- and pillar-type structures, and the results are plotted in Fig. 6 for s_0 values of 1, 0.1, and 0.01. For arrays of holes, the exposure is independent of s_0 if H/w is large (above 50) and increases with decreasing s_0 if H/w is small. This result is in agreement with the earlier work by Elam *et al.*[13] and Knoops *et al.*,[22] where the reaction-limited (small H/w) and diffusion-limited (large H/w) regimes were distinguished. For structures with a small H/w ratio, the limiting factor during the deposition will be the sticking probability. For larger H/w ratios, the geometry will be the limiting factor for the diffusion of the precursor molecules into the structure and the initial sticking coefficient will no longer influence the required exposure. For arrays of pillars, we observe that the required exposure is dependent of s_0 over the whole H/w range, suggesting a reaction-limited regime. As a consequence of the different dependency, the difference in required exposure for pillar- versus hole-structures becomes smaller with decreasing initial sticking coefficient. For a s_0 value of 0.1 [0.01], we find a factor around 3 [2]. It is expected that for even lower values of s_0, a regime is reached where the required exposure time will no longer depend on the geometry (hole versus pillar), but will solely be determined by the sticking probability.

In addition to the required exposure, the 3D MC model can also provide insights in the effective use of ALD precursors. The precursor efficiency can be calculated as the ratio between the number of chemisorbed and simulated MC particles. Figure 7 displays the precursor efficiency for the simulated exposures depicted in Fig. 6. It is clear that the lower required exposure for the arrays of pillars comes together with a significantly more efficient precursor usage, thus making these 3D structures much more ALD-friendly.
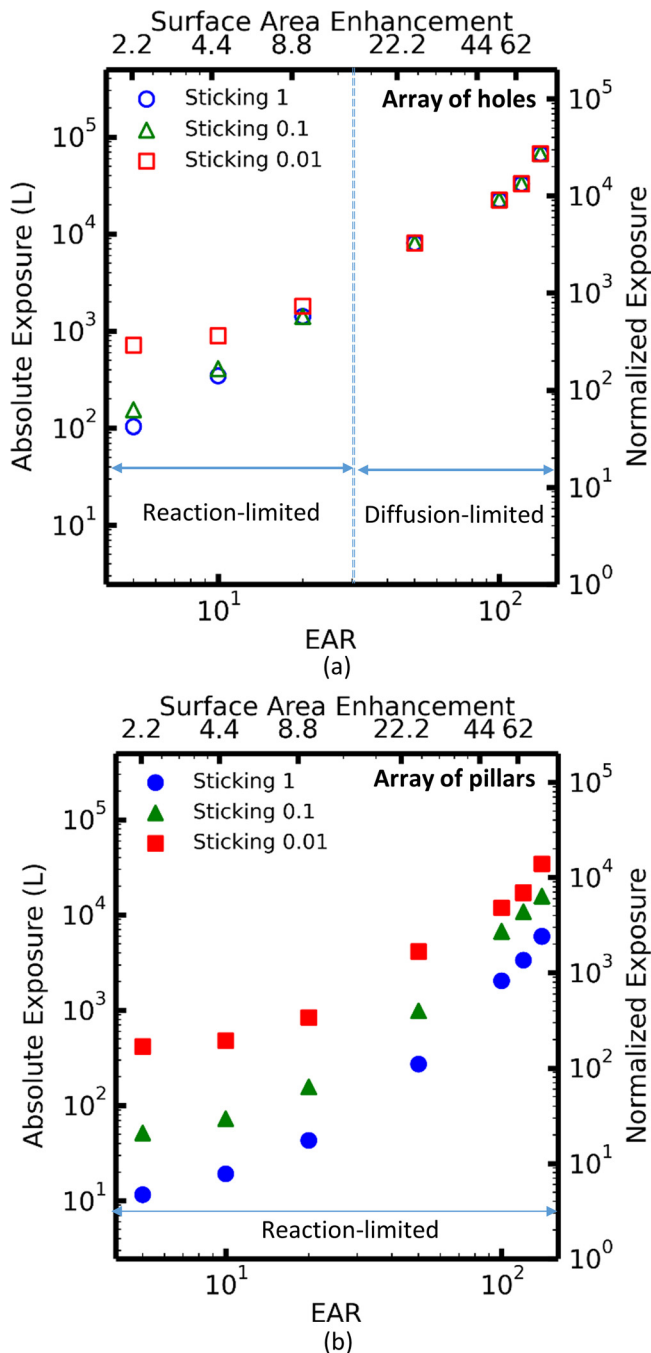

FIG. 6. (Color online) Cross section along the dashed horizontal lines in the color plots in Fig. 3 (data points for $s_0 = 1$). Required TMA exposure (left y-axis) and normalized exposure (right y-axis) as a function of the H/w ratio of arrays of holes and pillars with a fixed D/w ratio of 3 and for initial sticking probabilities, s_0, of 1, 0.1, and 0.01.
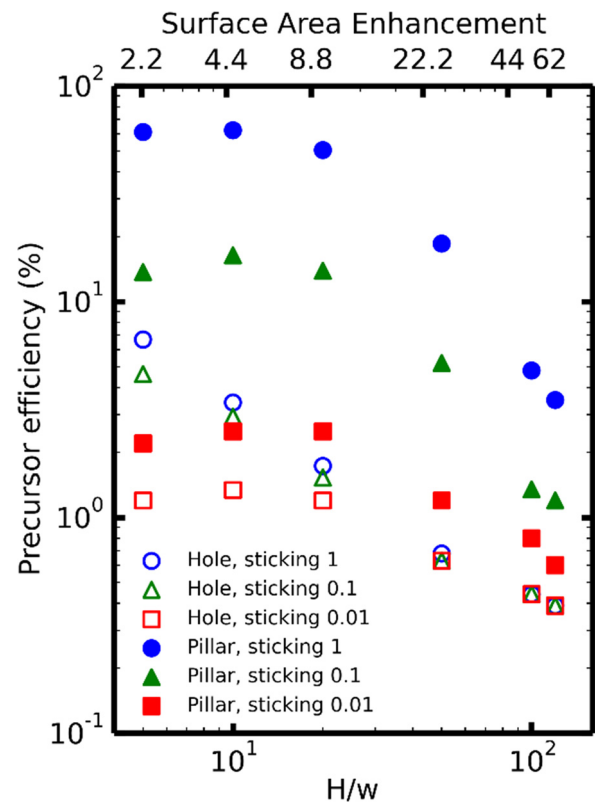

FIG. 7. (Color online) Precursor efficiency as a function of the H/w ratio of arrays of holes and pillars with a fixed D/w ratio of 3 and for initial sticking probabilities, s_0, of 1, 0.1, and 0.01.

IV. SUMMARY AND CONCLUSIONS

In this paper, we developed a full 3D Monte Carlo model to compare ALD on two different types of large surface area substrates: arrays of holes versus arrays of pillars. We found that, for initial sticking coefficients of 0.01 and higher, the exposure needed for conformal coverage of an equal surface area is larger for hole-type arrays than for pillar-type ones. The exposure for both structures becomes similar in the limit of small center-to-center distances of the pillars. Moreover, when targeting the same surface area enhancement factor, the precursor efficiency is significantly larger for a well-spaced pillar geometry than for a hole geometry with the same height to width ratio. Therefore, arrays (or "forests") of pillars are more suitable for ALD-based functionalization toward applications where large surface areas are desired, such as in sensors, solar cells, fuel cells, and batteries.

ACKNOWLEDGMENTS

[1]L. Puurunen, J. Appl. Phys. **97**, 121301 (2005).

[2]M. Ritala, M. Leskelä, J.-P. Dekker, C. Mutsaers, P. J. Soininen, and J. Skarp, Chem. Vap. Deposition **5**, 7 (1999).

[3]J. A. van Delft, D. Garcia-Alonso, and W. M. M. Kessels, Semicond. Sci. Technol. **27**, 074002 (2012).

[4]J. W. Elam *et al.*, J. Nanomater. **2006**, 1.

[5]M. Roberts *et al.*, J. Mater. Chem. **21**, 9876 (2011).

[6]C. Detavernier, J. Dendooven, S. P. Sree, K. F. Ludwig, and J. A. Martens, Chem. Soc. Rev. **40**, 5242 (2011).

[7]B. Min *et al.*, J. Cryst. Growth **252**, 565 (2003).

[8]Y.-C. Liang, C.-C. Wang, C.-C. Kei, Y.-C. Hsueh, W.-H. Cho, and T.-P. Perng, J. Phys. Chem. C **115**, 9498 (2011).

[9]S. Deng, S. W. Verbruggen, Z. He, D. J. Cott, P. M. Vereecken, J. A. Martens, S. Bals, S. Lenaerts, and C. Detavernier, RSC Adv. **4**,11648 (2014).

[10]S. K. Cheah *et al.*, Nano Lett. **9**, 3230 (2009).

[11]C. Liu, E. I. Gillette, X. Chen, A. J. Pearse, A. C. Kozen, M. A. Schroeder, K. E. Gregorczyk, S. B. Lee, and G. W. Rubloff, Nat. Nanotechnol. **9**, 1031 (2014).

[12]R. G. Gordon, D. Hausmann, E. Kim, and J. Shepard, Chem. Vap. Deposition **9**, 73 (2003).

[13]J. W. Elam, D. Routkevitch, P. P. Mardilovich, and S. M. George, Chem. Mater. **15**, 3507 (2003).

[14]T. Keuter, N. H. Menzier, G. Mauer, F. Vondahlen, R. Vaßen, and H. P. Buchkremer, J. Vac. Sci. Technol., A **33**, 01A104 (2015).

[15]A. Yanguas-Gil and J. W. Elam, J. Vac. Sci. Technol., A **30**, 01A159 (2012).

[16]A. Yanguas-Gil and J. W. Elam, Theor. Chem. Acc. **133**, 1465 (2014).

[17]G. Mazaleyrat, A. Estève, L. Jeloaica, and M. Djafari-Rouhani, Comput. Mater. Sci. **33**, 74 (2005).

[18]V. Dwivedi and R. A. Adomaitis, ECS Trans. **25**, 115 (2009).

[19]R. A. Adomaitis, Chem. Vap. Deposition **17**, 353 (2011).

[20]A. Holmqvist, T. Törndahl, and S. Stenström, Chem. Eng. Sci. **96**, 71 (2013).

[21]J. Dendooven, D. Deduytsche, J. Musschoot, R. L. Vanmeirhaeghe, and C. Detavernier, J. Electrochem. Soc. **157**, G111 (2010).

[22]H. C. M. Knoops, E. Langereis, M. C. M. van de Sanden, and W. M. M. Kessels, J. Electrochem. Soc. **157**, G241 (2010).

[23]J. Musschoot, J. Dendooven, D. Deduytsche, J. Haemers, G. Buyle, and C. Detavernier, Surf. Coat. Technol. **206**, 4511 (2012).

[24]N. Yazdani, V. Chawla, E. Edwards, V. Wood, H. G. Park, and, I. Utke, Beilstein J. Nanotechnol. **5**, 234 (2014).

[25]R. E. Cunningham and R. J. J. Williams, *Gasdiffusion: Diffusion in Gases and Porous Media* (Plenum, New York, 1980).

[26]A. Hasper, J. Holleman, J. Middelhoek, C. R. Kleijn, and C. J. Hoogendoorn, J. Electrochem. Soc. **138**, 1728 (1991).

[27]A. Kersch and W. J. Morokoff, *Transport Simulation in Microelectronics* (Birkhäuser, Basel 1995).

[28]J. Dendooven, D. Deduytsche, J. Musschoot, R. L. Vanmeirhaeghe, and C. Detavernier, J. Electrochem. Soc. **156**, P63 (2009).